



This is a repository copy of *Ultrasonic measurement for surface damage monitoring in coated bearing shells*.

White Rose Research Online URL for this paper:  
<https://eprints.whiterose.ac.uk/221326/>

Version: Published Version

---

**Article:**

Wu, L., Palamarciuc, I., Bajwa, R. et al. (2 more authors) (2024) Ultrasonic measurement for surface damage monitoring in coated bearing shells. *Friction*. ISSN 2223-7690

<https://doi.org/10.26599/frict.2025.9441065>

---

**Reuse**

This article is distributed under the terms of the Creative Commons Attribution (CC BY) licence. This licence allows you to distribute, remix, tweak, and build upon the work, even commercially, as long as you credit the authors for the original work. More information and the full terms of the licence here:  
<https://creativecommons.org/licenses/>

**Takedown**

If you consider content in White Rose Research Online to be in breach of UK law, please notify us by emailing [eprints@whiterose.ac.uk](mailto:eprints@whiterose.ac.uk) including the URL of the record and the reason for the withdrawal request.



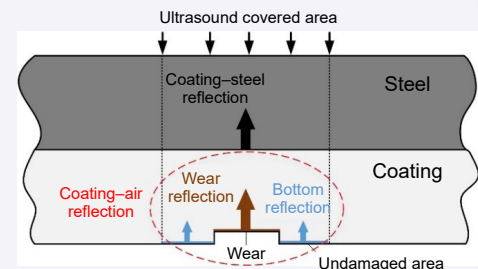
[eprints@whiterose.ac.uk](mailto:eprints@whiterose.ac.uk)  
<https://eprints.whiterose.ac.uk/>

# Ultrasonic measurement for surface damage monitoring in coated bearing shells

Liquan Wu<sup>1</sup>, Ion Palamarciuc<sup>2,✉</sup>, Rizwan Bajwa<sup>2</sup>, Yi Zhang<sup>3</sup>, Rob Dwyer-Joyce<sup>1,✉</sup>

**Cite this article:** Wu LQ, Palamarciuc I, Bajwa R, et al. *Friction* 2025, **13**: 9441065. <https://doi.org/10.26599/FRICT.2025.9441065>

**ABSTRACT:** Aluminium and other soft metal coated plain bearings are common in high-speed rotating machines due to their light weight and high performance. This makes the monitoring of bearing surface condition an important requirement to ensure healthy machine operation. In this paper, an ultrasound-based technique is investigated to measure the wear condition of thin aluminium bearing coatings. High-frequency 22 MHz piezoelectric sensors were selected based on both numerical simulations and experiments. Tests were performed on four groups of samples with artificial damage and three groups of samples worn by dry running. The results have shown the deviation between ultrasound measurement and microscope measurement are within 5  $\mu\text{m}$  for artificially damaged samples and within 15  $\mu\text{m}$  for samples worn under dry running conditions.



**KEYWORDS:** ultrasound measurement; piezoelectric sensors; surface wear diagnosis; plain bearing; aluminium coating material

## 1 Introduction

Plain bearings and bearing shells are widely used as key parts of rotary machines, such as the bushings in a combustion engine or the stern tube bearing in marine vessels. During their operation, the surface of shell is subjected to wear, damage, and fatigue, which requires the application of coating materials to provide a protective low friction layer. Generally, bearing shell failure starts with wear or surface damage of the coating material. It would be beneficial to the industrial field if the surface damage can be identified before the actual bearing failure.

Existing non-destructive testing methods for a bearing system focus on a specific issue, such as temperature, wear debris, vibration levels, or oil film properties between the shaft and bearing. The condition of the system or the failures can be speculated by the change of these issues. For example, temperature is related to heating from over-load or high friction, so Glavatskih [1] evaluated the oil film condition by monitoring the temperature change. Vibration and acoustic emission (AE) are two common methods for monitoring the operation status of a bearing system, especially a roller bearing or a ball bearing [2–4]. The shock wave led by the excessive load or friction of the element-race contact will be captured by the vibration or AE sensors, which is used to distinguish oil contamination, starvation, and the change of lubrication regime [5–7]. In a journal bearing or plain bearing system, the lubrication regime can be estimated through vibration

and AE signals, because of the variation of the film and friction [8, 9]. For example, when there is oil starvation, an excessive load or a speed drop-down, the friction state or lubrication regime of the bearing-shaft contact will shift from hydrodynamic to mixed, and even the boundary regime. The excessive friction can be seen as an abnormal signal with discrete frequency band or massive frequency shift in vibration or AE measurement [10, 11]. For the vibration or AE-based measurement, various sensors have been applied, such as accelerometers, laser scanning sensors, and eddy-current sensors [12–14]. The above techniques require the sensors to be mounted outside the device or bearing system, which may be easily affected by the ambient conditions.

The change of lubrication condition or clearance is also shown as a variation in oil film thickness. When there is an oil film thickness change led by a bearing failure, the capacitance and the ultrasonic properties of the oil film will be affected, and the oil film thickness can be measured by this variation [15, 16]. Ultrasound reflectometry has been reported effective in measuring circumferential oil film thickness when a shaft is spinning, through a series of shaft-mounted sensors [17, 18]. However, the researches and findings above are mainly interested in operational changes in bearing behaviour during or after the failure, which means those properties to be measured are changed after the bearing surface deformation or damage. Therefore, a method that can monitor the thickness of the bearing coating directly will avoid the subsequent abnormal operation.

<sup>1</sup> Leonardo Centre for Tribology, Department of Mechanical Engineering, The University of Sheffield, Western Bank, Sheffield S10 2TN, UK. <sup>2</sup> Daido Metal Co., Ltd. European Technical Centre (UK), Ilminster Somerset TA19 9PH, UK. <sup>3</sup> Daido Metal Co., Ltd. Technology Division, Tendoh Shinden, Maehara, Inuyama, Aichi 484-0061, Japan.

✉ Corresponding authors. E-mail: I. Palamarciuc, Ion.Palamarciuc@daidometal.com; R. Dwyer-Joyce, r.dwyer-joyce@sheffield.ac.uk

Received: June 29, 2024; Revised: December 19, 2024; Accepted: December 31, 2024

© The Author(s) 2025. This is an open access article under the terms of the Creative Commons Attribution 4.0 International License (CC BY 4.0, <http://creativecommons.org/licenses/by/4.0/>).

Regarding the wear or material loss, various approaches have been investigated, evaluated by some typical quantitative indicators including weight loss, relative displacement, out of roundness, clearance change, and wear debris [19–21]. When there is a material loss of bearing surface, the wear debris will lead to an induction change of the lubricant and the wear can be described through the variation of induction [22]. Similarly, the material loss also leads to the increase of oil film thickness, so that the wear status can be measured through the electro-magnetic or acoustic approaches [23]. Optical methods such as light sectioning, photo-metric stereo imaging have been used for the roughness and wear measurement of metallic materials [24, 25]. Three-dimensional optical profilometer, Raman spectroscopy, and high-speed imaging are also used to monitor the *in-situ* material wear process [26, 27]. In addition, a pin with fiber Bragg grating was mounted to a marine bearing to measure the wear status during friction [28]. For some underwater conditions, the ultrasound immersion measurement has been carried out on a series of objectives, such as polymer materials and additive manufactured coatings [29, 30]. However, these sensing techniques require sufficient space for the sensor mounting and can only be applied under laboratory conditions. The acoustic approaches have been investigated together with the machine learning methods, and the vibration and AE signals are analysed and evaluated by machine learning models [31, 32]. As passive testing approaches, the vibration or AE methods have significant limitations, one of which is lack of considering the impact of environmental factors in actual bearing systems, especially environmental noises.

Compared with other non-destructive methods, the advantage of ultrasound lies in its small sensor volume and robustness under electromagnetic interference. Ultrasound-based wear measurement has been carried out on a rotating disk, and the signal has been processed and analysed in the frequency domain [33, 34]. According to this research, the wear condition of the surface can be obtained by calculating the shift of resonance frequency or the phase shift of a certain frequency. However, when performing a frequency analysis, only the reflection pulse is analysed and it requires a high sample rate to contain sufficient points within a pulse, to enhance the frequency resolution. The trimmed length of the reflected signal will directly affect the frequency spectrum, which means that frequency domain analysis is difficult to achieve the measurement of dynamic variables, such as wear. In addition, the low-frequency ultrasound sensors were used under these circumstances, usually less than 10 MHz. In the manufacture of piezo-electric materials, a lower frequency corresponds to a thicker element, which will occupy a larger space for sensor mounting.

Therefore, this study seeks to demonstrate an ultrasound-based wear measurement method for practical application in aluminium alloy coated bearing shells. Considering the space and resolution, high-frequency piezo-electric sensors will be used in the measurement system, and time-domain analysis will be carried out to obtain the wear status of the coating material. This ultrasound solution will effectively reduce the volume of the sensor ( $\sim 2 \text{ mm} \times 1 \text{ mm}$ ) while ensuring high spatial resolution, making it suitable for real-time measurement and potentially applied in long-term monitoring, such as the stern tube bearings or main shaft bearings of large vessels.

## 2 Principles of ultrasound wear measurement

### 2.1 Ultrasound pulse-echo technique

In this study, ultrasound pulse-echo is used for the coating

measurement, and each sensor works as both signal transmitter and receiver. When the transmitted ultrasound meets the coating–steel interface and coating–lubricant interface, there will be two corresponding reflections. The coating thickness can be obtained by comparing the time-of-flight (ToF) of two reflected signals. The expression for coating thickness  $d$  is

$$d = c(T) \cdot \frac{\Delta t}{2} \quad (1)$$

where the speed  $c$  of sound is the function of temperature  $T$ , and  $\Delta t$  represents the ToF difference between the two reflections. The position of reflections is determined by the peak position of the reflection pulses.

### 2.2 Near field in ultrasound measurement

Pulse-echo technique is frequently used in ultrasound thickness measurement, and it has a good sensitivity to defects parallel with the surface. However, there is a “blind area” in front of the sensor, also known as the near field. The presence of a tiny feature in this area can cause a large reflection, and vice versa. The length of the near field  $N$  is expressed by

$$N = \frac{S_0 f}{\pi c} \quad (2)$$

where  $S_0$  is the area of the sensor and  $f$  is the frequency of ultrasound. Because of the existence of near field, when using ultrasound to measure the wear of coating, the two interfaces of the coating should locate out of the near field region.

## 3 Simulations of the interaction between ultrasound and wear

In actual operation, the surface of bearing coating is not always smooth, and the formation of wear always starts with some small scars or damage. Then, this small damage grows into a larger wear area. Moreover, the thickness of the coating material is typically less than  $500 \mu\text{m}$ , which is spatially difficult to resolve using low frequency ultrasound because of the near field effect. To explore these effects, a finite element method (FEM) has been applied to simulate the interaction between ultrasound and worn regions of coating, including the effect of a series of factors, such as the frequency of ultrasound, the size, and continuity of wear regions. In the simulations, two typical frequencies were investigated, 10 MHz, which is a common frequency band used in longitudinal ultrasound measurement, and 22 MHz, the common frequency band of high-frequency piezo-electric sensors.

### 3.1 Setup of the numerical model

A two-dimensional model has been built, which consists of an aluminium layer on a steel substrate to simulate a small area of a bearing component. Figure 1(a) shows the three-dimensional diagram of a bearing shell, with directions are marked, including three directions, width direction ( $z$ -direction in Fig. 1(a)), circumferential direction and depth direction. The two-dimensional model was built on the width and depth direction, as the  $yz$  plane in Fig. 1(a).

Figure 1 shows an undamaged example, which can be regarded as a cross-section perpendicular to the circumferential direction. The parameters used in the simulations are shown in Table 1. In Fig. 1, the blue lines represent the input area of ultrasound vibration vector  $\mathbf{F}$ , perpendicular to the interface. The amplitude is expressed as Eq. (3). PML stands for perfect matched layer, which is used to simulate an infinite space. In Eq. (3), the time

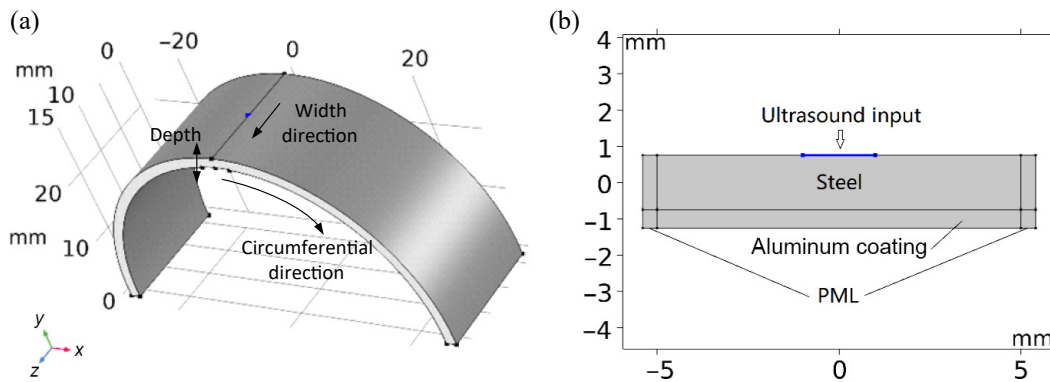


Fig. 1 Diagram of FEM modelling: (a) three-dimensional model showing reference direction; (b) two-dimensional model of an undamaged example.

Table 1 Properties of materials in FEM modelling

Description	Density (g/cm <sup>3</sup> )	Thickness (mm)	Width (mm)	Young's modulus (10 <sup>9</sup> Pa)	Poisson's ratio ratio
Aluminium coating layer	2.70	0.5	10	70	0.33
Steel bearing layer	7.85	1.5	10	205	0.28
Signal input region	—	—	2	—	—

step is in the range  $t \in [0, 3/f]$ , where  $f$  is the ultrasound frequency. The input region is also used as the probe to receive the reflected signals.

$$|\mathbf{F}| = \left(1 - \cos\left(\frac{2\pi ft}{3}\right)\right) \cdot \sin(2\pi ft) \quad (3)$$

Regarding the meshing, the density and size of the grid should change with the target frequency, so the meshing parameters should be different between 10 and 22 MHz simulations. However, when the frequency is lower, the wavelength will be larger, so the pre-set grid size under 22 MHz input condition is also available for 10 MHz input condition. Therefore, the pre-set grid size in Fig. 1 was set as from 10 to 50  $\mu\text{m}$ , with a smaller grid size at the corner area. And there were 1,616 units on the boundaries and 17,280 units inside the domain.

The governing equation of the elastic wave is given by

$$\frac{E}{2(1+\nu)} \left( \nabla^2 \mathbf{u} + \frac{1}{1-2\nu} \nabla(\nabla \cdot \mathbf{u}) \right) + \mathbf{F} = \rho \frac{\partial^2 \mathbf{u}}{\partial t^2} \quad (4)$$

where  $E$  is the Young's modulus;  $\nu$  is Poisson's ratio;  $\rho$  is the density of the media. The displacement and boundary pressure are in vector form,  $\mathbf{u}$  and  $\mathbf{F}$ . The zero initial displacement and zero velocity are set as boundary conditions.

### 3.2 Ultrasound frequency selection

A series of simulations was carried out to study the influence of ultrasound frequency on wave propagation in damaged aluminium layers. Two common ultrasound frequencies, 10 and 22 MHz were investigated, the ultrasound incident region was kept at 2 mm along the width direction and the dimension of wear/damage was 2 mm in width and 0.1 mm in depth (2 mm  $\times$  0.1 mm) in each case.

The frequency simulation results are shown in Fig. 2. Figure 2(a) shows the propagation of 10 MHz ultrasound signals in a 1.5 mm thick steel component with a 0.5 mm aluminium coating and Fig. 2(b) shows the 22 MHz signal response of the same structure.

The reflections of 10 MHz ultrasound signal from the two interfaces (Fig. 2(a)) are too close to be distinguished, especially for the damaged conditions. In comparison to a 10 MHz signal, a

22 MHz signal response (Fig. 2(b)) has a better visual result, and the two reflections from two coating interfaces can be easily separated. Therefore, 22 MHz ultrasound was initially selected as the central frequency for sensor instrumentation due to its higher spatial resolution.

### 3.3 Interaction between ultrasound and wear

A wear damaged bearing surface could manifest as large material removal or a region of small discrete scars. For example, when there is an excessive load or friction, a massive amount of coating material will be peeled off from the surface, as the "large material removal" in Fig. 3(a). And when there are some hard particles or asperity contacts while shaft is spinning, the surface damage is shown as some tiny grooves along the rotation direction, as the "discrete scars" in Fig. 3(b).

Two different simulations using 22 MHz ultrasound have been performed to simulate these two conditions. A material-removed region (4 mm wide and 0.1 mm deep) was established (Fig. 3(a)), to simulate a large wear damage. A simulation with two 0.5-mm-wide scars (Fig. 3(b)) was used to analyse the response from small discontinuous damage. The results are shown in Figs. 3(c) and 3(d) respectively and the time-of-arrival (TOA) of the reflections is marked.

According to the results in Fig. 3(c), when the area of damage is larger than the area of ultrasound input region, the ultrasound signal is fully reflected at the wear scar. The reflection of the coating-air interface has moved leftwards, which means the reflection from the wear arrives earlier than the one from an undamaged surface. For discontinuous wear scars (Fig. 3(d)), there are two reflections from the coating-air interface, one of which is from the thinner area (damaged area), while the other is from the undamaged area, as marked areas A and B.

Further simulations were carried out to study the effect of wear scar width. In Fig. 4(a), the signal response from a 2 mm-wide scar (blue) is compared with that from an undamaged surface (red, reference), which is the zoomed reflection area of Fig. 2(b). It is worth noting that in this case, the width of the wear, 2 mm, is the same with the width of ultrasound input region. It shows the same pulse shape with Fig. 3(c), the result from a 4-mm-wide scar, which means the 2 mm ultrasound applied region can fully receive the reflection from the scar with the same size.

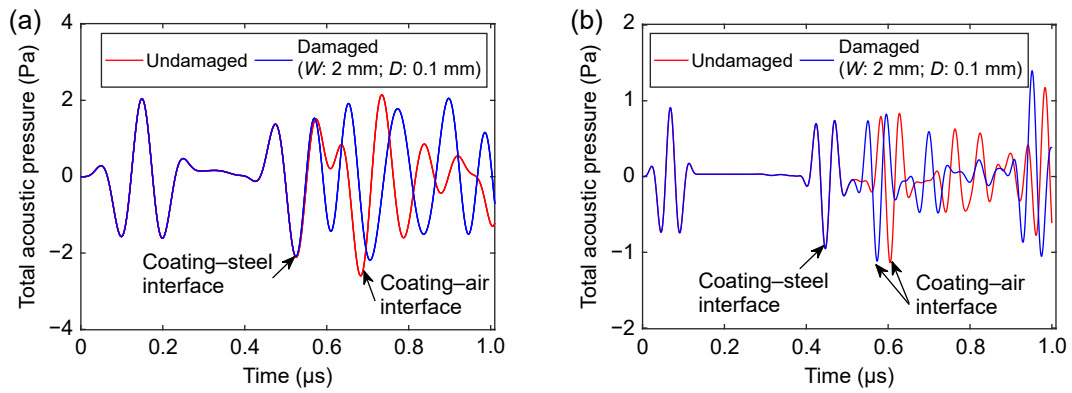


Fig. 2 Simulation results for ultrasound frequency selection for undamaged (red) and damaged 2 mm × 0.1 mm samples (blue): (a) 10 MHz, and (b) 22 MHz transducer.

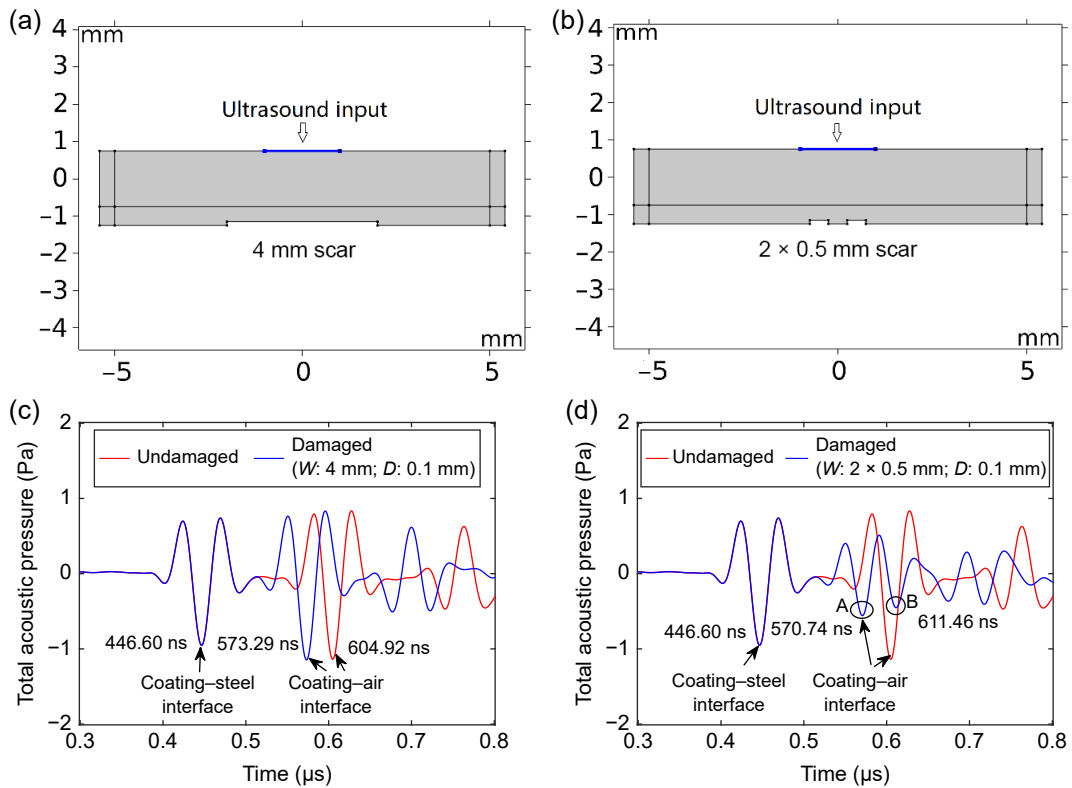


Fig. 3 Simulation of the interaction between ultrasound and (a) a 4-mm-wide wear scar, and (b) two discontinuous 0.5-mm-wide wear scars. The simulation results for an (c) 4-mm-wide scar and (d) two 0.5-mm-wide scars: undamaged (red) and damaged (blue).

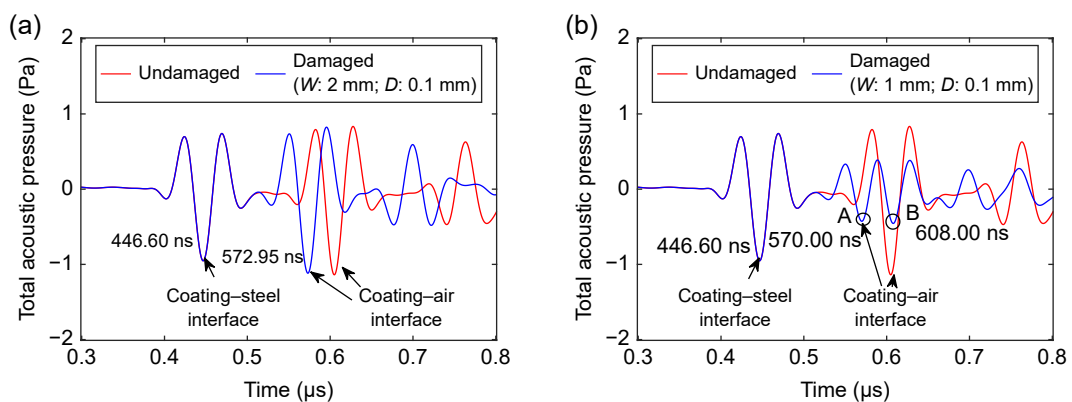


Fig. 4 Simulation results for an undamaged (red) and damaged sample with 0.1-mm-deep flat scar (blue): (a) 2-mm-wide, and (b) 1-mm-wide scars.

Figure 4(b) shows the reflection from a 1-mm-wide scar, which has a similar shape to the signal in Fig. 3(d), the reflection from two separate 0.5-mm-wide scars. It means that during the measurement, the ultrasound is sensitive to the thickness change of the coating, but cannot determine whether this kind of change is continuous or not.

Comparing the results in Figs. 4(a) and 4(b), there is an extra dip (marked as A and B in Fig. 4(b)) when the size of the damage is smaller than the ultrasound input area. This is caused by the superposition of the reflections from the damaged and undamaged area, as shown in Fig. 5.

Because the ultrasound travels in the form of a plane wave, when it contacts the wear, it will be reflected as shown in the red “wear reflection” in Fig. 5, also shown as the dip A in Fig. 4(b). The remaining part will propagate to the undamaged surface and reflect as a “bottom reflection”, dip B in Fig. 4(b). Because the area of damaged surface is 1-mm-wide which is equal to the width of undamaged area, the amplitudes of dips A and B are almost the same. It means that when the wear depth is constant, the larger the width of wear, the greater the amplitude of its reflected signal. The deeper the wear depth, the closer the reflected signal of the wear is to the coating steel reflection. This could be potentially used to determine damage regions of different wear dimensions. Moreover, when there is a large material removal, if the ultrasound sensor locates above that area, the material loss could be measured and the reflection signal of coating–air interface will show as an independent pulse. When there are some small and discrete scars, the ultrasound could still measure the damage, but the reflection will be a superposition of two adjacent reflections.

Based on the simulation results, it can be concluded that the thickness of the coating can be measured through the difference of the TOA between the two reflections from the two interfaces of the coating, also known as the ToF of the ultrasound signal. The coating thickness is calculated, using ToA marked in Figs. 3 and 4, and the speed of sound in pure aluminium is 6,300 m/s.

The simulated result shows a slight difference with the pre-set value during the modelling (Table 2). When there are some different thickness levels, as the 2× 0.5 mm-wide scar model and 1 mm-wide scar model, the reflected signals display as several

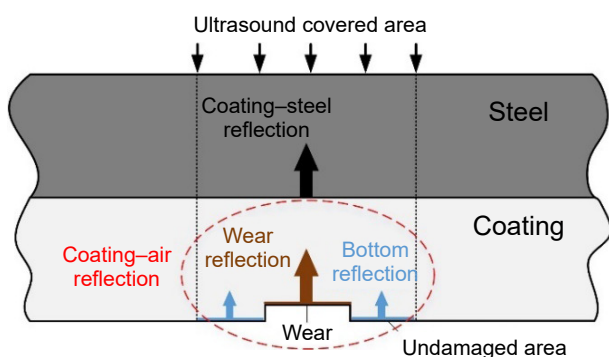


Fig. 5 Reflections at coating–steel interface and coating–air interface.

peaks or dips, where the first to arrive corresponds to the minimum coating thickness (maximum wear). For example, in the 2× 0.5 mm-wide model, the minimum coating thickness is calculated as 391.04 μm, while the pre-set thickness is 400 μm. The wear condition can be obtained by comparing the initial thickness and the thickness during measurement. In the 2× 0.5 mm-wide model, the measured wear value 108.96 μm is slightly higher than the pre-set wear value 100 μm. In the further practical ultrasound test, the measurement and post-process can follow the same procedure, using ToF between the two coating interface reflections to get the residual thickness and the wear is calculated by the difference between residual thickness and initial thickness.

## 4 Experimental ultrasound measurements

### 4.1 Test system set-up and instrumentation

Figure 6 shows the design of the ultrasound testing system for wear measurement of aluminium alloy-coated bearing shells. The entire system is based on an ultrasound pulse-echo technique. The data from ultrasound sensor was collected by a digital oscilloscope, which was then transmitted back to a computer and recorded. A digital oscilloscope PicoScope was used for transmitting and receiving electrical signals, and a digital acquisition (DAQ) card TC-08 was used to acquire temperature signals for a K-type thermocouple. A virtual instrument based on LabVIEW was designed to control the above components.

According to the simulation results described above, for the aluminium coating with a thickness of about 500 μm, 22 MHz ultrasound is a suitable choice for measurement of the thin metallic coating with and without wear damage. The piezoelectric material DL50-HD from DEL Piezo Ltd. was selected, which will work both as a transmitter and a receiver during the test. The main characteristics of DL50-HD are shown in Table 3. The size of ultrasound sensor is approximately 2 mm × 1 mm to accommodate the curvature of the outer surface of the bearing shell.

### 4.2 Speed of sound calibration

Ultrasound pulse-echo testing was used to calibrate the speed of sound of the aluminium alloy coating. In the speed of sound calibration, the test samples were heated in a programmable oven and the ToF data were recorded with the temperature change. After test, the calibration sample was sectioned, and its thickness was measured through cross-section graphing. Finally, the speed of sound variation with temperature was derived through the thickness and ToF change with temperature. The variation was close to linear, and a simple curve fit was applied:

$$c_{Al}(T) = -2.26 \times T + 6477 \tag{5}$$

where  $c_{Al}$  is the speed of sound in the aluminium alloy coating material and  $T$  is the temperature.

Table 2 Calculation of coating thickness in FEM modelling

	ToF between reflections (ns)	Simulated ultrasound result (μm)	Preset thickness value (μm)
Undamaged model	158.32	498.71	500
W: 4 mm; D: 0.1 mm	126.68	399.04	400
W: 2× 0.5 mm; D: 0.1 mm	124.14/164.86	391.04/519.31	400/500
W: 2 mm; D: 0.1 mm	126.35	398.00	400
W: 1 mm; D: 0.1 mm	123.40/161.40	388.71/508.41	400/500

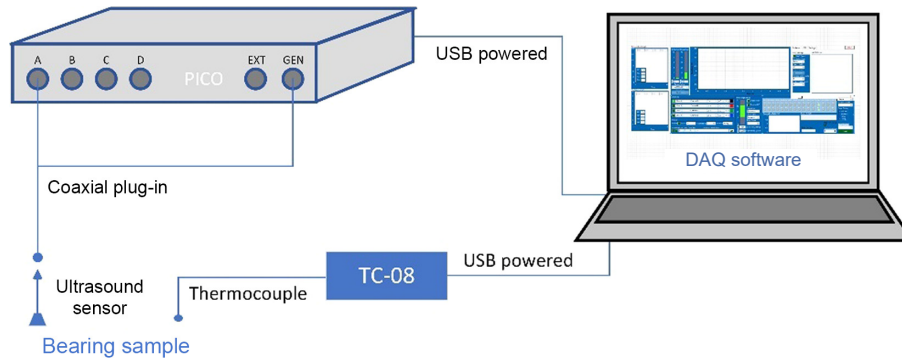


Fig. 6 Diagram of ultrasound bearing shell measurement system.

Table 3 Material properties of DL50-HD

Property	Strain constant, $d_{33}$ ( $10^{-12}$ C/N)	Voltage constant, $g_{33}$ ( $10^{-3}$ V·m/N)	Relative dielectric constant, $\epsilon$ (free/clamp)	
Value	430	25	1,950/890	
Property	Electromechanical coupling factor, $K$	Quality factor, $Q_m$	Density, $\rho$ ( $\text{g}/\text{cm}^3$ )	Curie point, $T_c$ ( $^\circ\text{C}$ )
Value	0.49	35	7.9	365
Property	Speed of sound, $C_L$ (m/s)	Acoustic impedance, $Z$ (MRayl)	Frequency constant at thickness mode, $N_t$ (MHz·mm)	
Value	2,860	23	2.03	

## 5 Ultrasound measurement using different frequency sensors

### 5.1 Test description

Figure 7 depicts the layout of the instrumented bearing shells, with one sensor mounted at the axial centre on the tab side (sensor 1) and the other was mounted onto the top centre (sensor 2) as shown. Both 10 and 22 MHz sensors were installed on shells in this configuration. The white dash lines show the cutting location for the cross-section measurement.

During testing, a single cycle sine pulse with a frequency equal to the centre frequency of the sensor was used as the test input signal to perform A-scan detection on samples. 100 sets of A-scans were collected for each test under room temperature, about  $20 \pm 1$   $^\circ\text{C}$  measured by the thermocouple, bonded onto the steel substrate of shell, and the sound speed of aluminium alloy coating was 6,430 m/s. A low-pass filter with 50 MHz cut-off frequency was applied after data collection, to eliminate electrical noise. A spline interpolation was used to enhance the resolution, which raised the sampling interval from 2 to 0.2 ns.

### 5.2 Results

According to Fig. 5, the first reflection should be composed of two independent reflections, the coating–steel interface reflection and coating–air interface reflection. However, in actual measurements (Fig. 8), the response of the 10 MHz sensors showed an unsatisfactory performance, with two reflections completely mixed. The first reflection was about to overlap with the second reflection at about 1.9  $\mu\text{s}$ . From this kind of waveform, it is difficult to separate the signals of the two interfaces of the aluminium alloy coating. So, it is unfeasible to use a 10 MHz sensor to detect the thickness of the coating at the micron level.

The 22 MHz sensors (Fig. 9) show a clearer reflection pattern. The two reflections from coating interfaces are distinctive, with the coating–steel and coating–air interfaces marked in the figures. In addition, second reflection inside coating was observed. It is worth noting that the term “secondary reflection inside coating” here is different from the previous “second reflection”. “Second



Fig. 7 Undamaged aluminium alloy-coated bearing shell and layout of sensors for ultrasound frequency tests.

reflection inside coating” refers to the signal formed by each overall reflection of ultrasound at the coating–air interface but reflected twice inside the coating. Theoretically, the distance along the  $x$ -axis (ToF) between the three peaks marked in Figs. 9(a) and 9(b) should be equal, which represents the duration of ultrasound traveling back and forth inside the coating.

Using the ToA between two coating interfaces, the ToF can be calculated by comparing the ToA difference in each group. The results of ultrasound measurement with 22 MHz sensors are compared with microscope measurements of the coating thickness recorded after the shell was sectioned, as shown in Table 4. Figures 10(a) and 10(b) show an example cross-section of the shell and coating. The 22 MHz ultrasound shows excellent accuracy on measuring an undamaged coating, with a 1% relative error.

## 6 Measurement of bearing shells with artificial damage

### 6.1 Test description

Four artificially damaged bearing shells were studied. The middle and tab sides of each sample were machined with a groove by electrical discharge machining (EDM). For each sample, six ultrasound sensors were mounted on the surface of the bearing, with sensor positions shown in Fig. 11(a). The white dash lines represent the location of the cross-section measurement. Two of

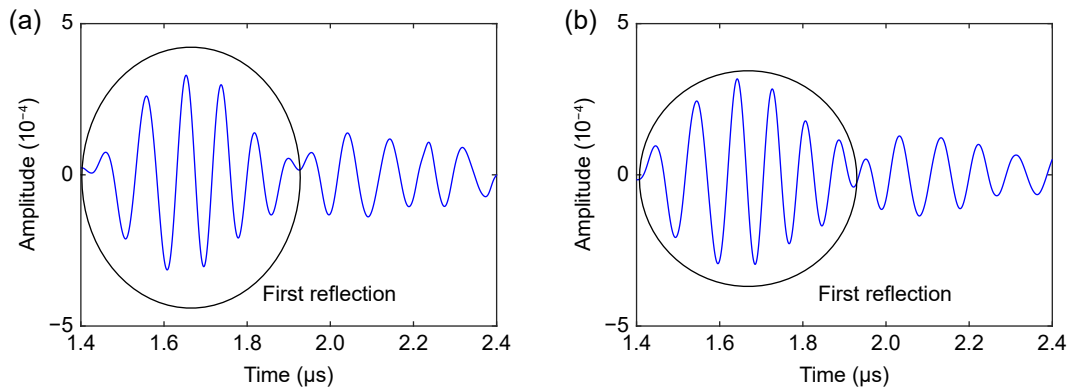


Fig. 8 Waveform of first reflection of 10 MHz: (a) sensor 1; (b) sensor 2.

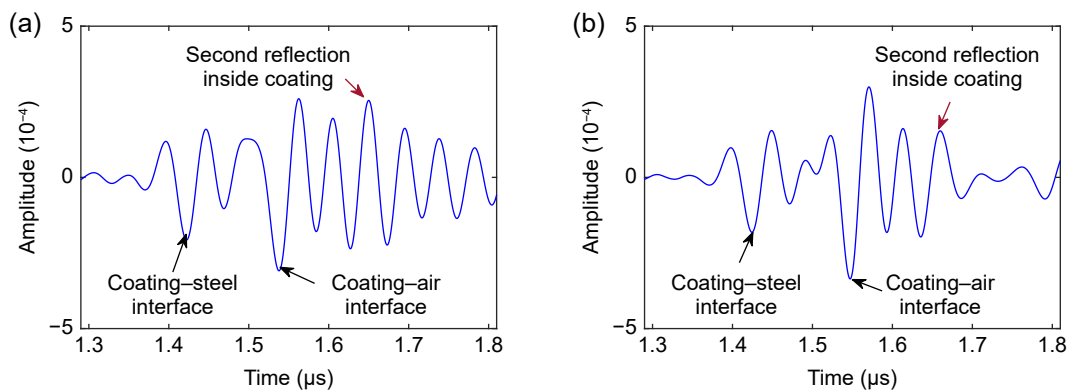


Fig. 9 Waveform of first reflection of 22 MHz: (a) sensor 1; (b) sensor 2.

Table 4 Measurement results of aluminium alloy coating using 22 MHz sensors

	Sensor 1	Sensor 2
ToF between interfaces (ns)	115.618	122.728
Thickness from ultrasound ( $\mu\text{m}$ )	371.71	394.57
Thickness from microscope ( $\mu\text{m}$ )	368.04	393.78
Deviation ( $\mu\text{m}$ )	3.67	0.79
Error	1.00%	0.20%

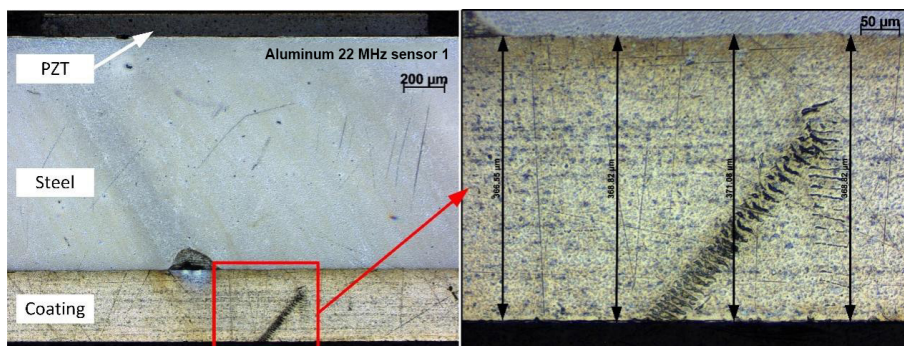


Fig. 10 Global cross-section view of ultrasound measured coating and its thickness measurement (22 MHz sensor 1).

the sensors were applied above the damage in the middle (sensors 3 and 4), two have been mounted above the tab-side damage (sensors 1 and 2), and remaining (sensors 5 and 6) were set on the other side symmetrical to the tab-side damage, but covering the undamaged area. Among these samples, two samples were subjected to artificial damage of about 50  $\mu\text{m}$  in depth, and the remaining samples had nominal damage values of 100 and 150  $\mu\text{m}$  in depth, respectively. The location of the damage regions is shown in Fig. 11(b).

Figures 11(c) and 11(d) show example cross-section images of two different sensor test areas on aluminium alloy coated sample 1 (50  $\mu\text{m}$ ): Fig. 11(c) the EDM processed area and Fig. 11(d) the un-processed area. The removed thickness 50  $\mu\text{m}$  is a nominal value, which means the actual thickness removed may not be exactly that value. Intuitively, compared to Fig. 11(c), Fig. 11(d) shows a thicker coating, smoother bottom surface, and a more uniform coating structure. It could be observed from the 20 $\times$  zoomed images that the surface treated with EDM is rougher than the

surface without treatment. So, if the thickness of the damaged coating can be measured by ultrasound and compared with the undamaged result, the thickness removed by EDM can be estimated.

### 6.2 Results

Figure 12 shows examples of ultrasound reflections and ToA curves of the four artificially damaged samples. The two dips correspond to the two reflections from coating-steel interface and

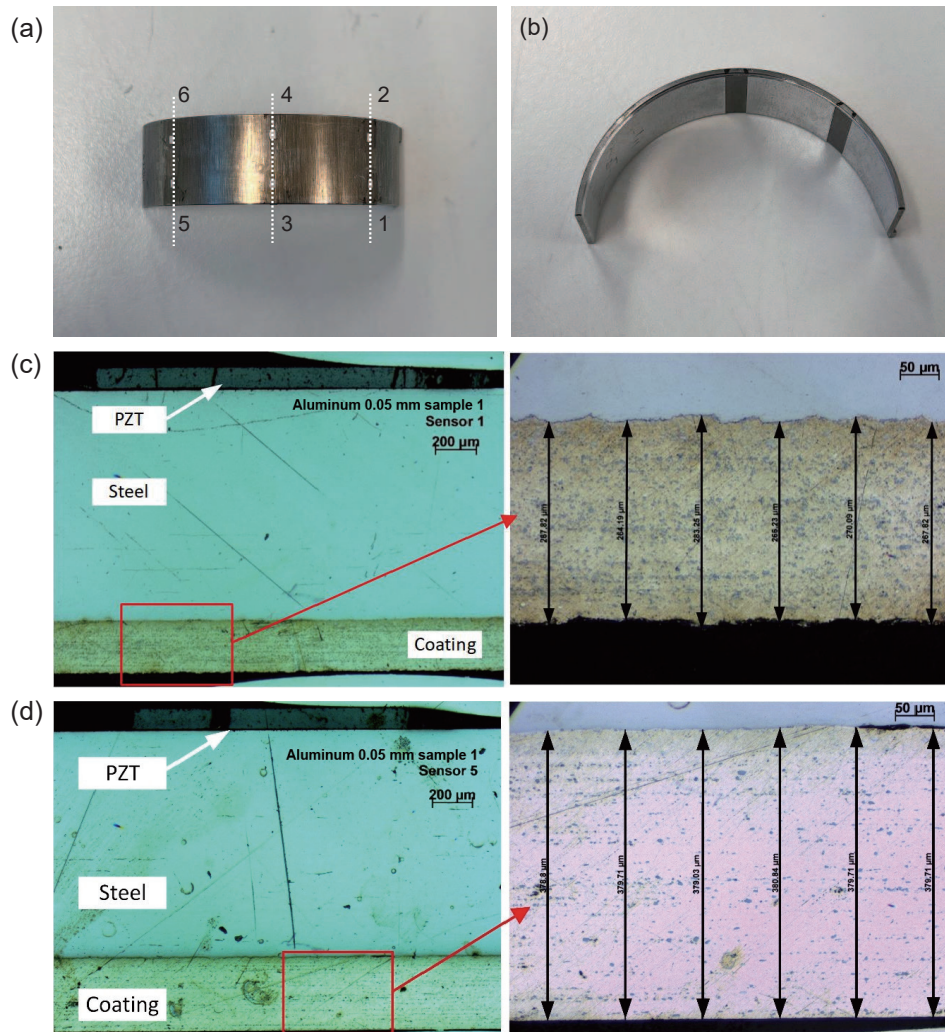


Fig. 11 Example of aluminium alloy-coated bearing shell Sample 1 with artificial damages: (a) layout of sensors; (b) artificial damages on the inner surface; global cross-section view (5× objective) and the thickness measurement (20× objective) of (c) sensor 1 and (d) sensor 5.

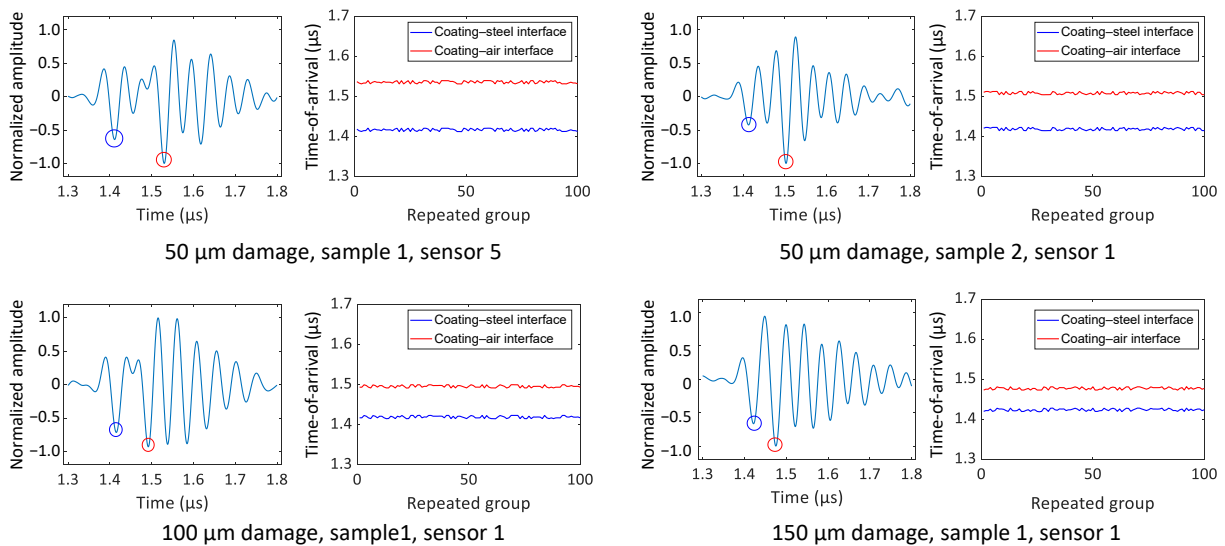


Fig. 12 Examples of ultrasound reflection and ToA curves for artificial damages.

coating-air interface, which are marked in blue and red respectively. The blue and red line in the ToA curves represent the ToA of the two interface reflections and the 100 repeated groups stand for the 100 A-scans. Sensor 5 of the 50 μm Sample 1 is shown as the result of undamaged surface. From Fig. 12, when the wear is deeper, the two reflection dips are becoming closer, which is the same as the ToA curves.

Tables 5(a)–5(d) show the ultrasound results of four artificially damaged samples compared with the microscope results. Both show a similar trend, and the deviation between them was less than 5 μm in each case. The undamaged coating thickness under sensors 5 and 6 areas was taken as the reference, then for 50 μm wear sample 1, ultrasound testing shows that the damage depth of the actual bearing surface is 99.25 μm, while the damage depth calculated from the microscope results is 98.62 μm, as shown in Table 5. Similarly, for 50 μm wear sample 2, ultrasound testing showed that the damage depth of the actual bearing surface was 76.74 μm, while the damage depth calculated from the microscope results was 80.05 μm. The results are in good agreement, and it is clear that whilst the target machining depth was 50 μm, the final value achieved was much greater. Both the other two sets of data (Table 5(e)) show that in these cases the machined depth was also greater than intended.

The depth prediction accuracy is encouraging and demonstrates that ultrasound shows potential in the wear detection of aluminium alloy coatings, which can effectively detect 100–200 μm artificial surface damage on a 370-μm-thick

aluminium alloy coating. In terms of thickness measurement, the ultrasound results are very close to those of microscope, with a general deviation around 5 μm and a maximum deviation of 13.75 μm (7.42% relative error).

## 7 Dry-running test on a bearing shell

### 7.1 Test description

In this evaluation a bearing sample was run under dry (no lubricant) running conditions to rapidly generate wear. The shell was instrumented with fourteen 22 MHz ultrasound sensors. Before the operation, the ultrasound signals of each sensor were collected and used as reference signals for further wear measurement. Subsequently, the bearing shell with sensors was installed onto the rotary machine through a bearing holder. The model of machine is Rotary Tribometer TE92 from Plint Technology, as shown Fig. 13(a).

The duration of operation was 10 min, the load provided by TE92 was 0.2 kN, and the rotation speed was set at 730 r/min. The bearings were disassembled from the rig after cooling down, and isopropanol was used to flush and remove the wear debris on the inner surface. Then, the ultrasound signals were recorded after the flushing procedure, using some temporarily connected coaxial wires. The data were collected after the shell was fully cooled down. So, it can be regarded the heat of coating has been fully exchanged with the steel and the temperature between coating and steel can be regarded as the same, which was 20±1°C

**Table 5** Measurement results of aluminium alloy coated bearings ((a) 50 μm damage, sample 1; (b) 50 μm damage, sample 2; (c) 100 μm damage, sample 1; (d) 150 μm damage, sample 1; (e) comparison of damage depth between ultrasound and microscope testing)

(a)	Sensor 1	Sensor 2	Sensor 3	Sensor 4	Sensor 5	Sensor 6
ToF between reflections (ns)	86.44	85.90	86.75	88.60	118.87	116.72
Thickness from ultrasound (μm)	277.92	276.17	278.91	284.85	382.17	375.25
Thickness from microscope (μm)	273.21	274.00	280.51	288.97	380.28	375.31
Deviation (μm)	4.70	2.17	1.60	4.12	1.88	0.06
Error	1.72%	0.79%	0.57%	1.42%	0.49%	0.02%
(b)	Sensor 1	Sensor 2	Sensor 3	Sensor 4	Sensor 5	Sensor 6
ToF between reflections (ns)	89.70	93.12	86.47	87.01	115.50	110.39
Thickness from ultrasound (μm)	288.40	299.39	278.00	279.75	371.35	354.90
Thickness from microscope (μm)	288.02	295.93	273.40	282.03	369.99	359.79
Deviation (μm)	0.38	3.46	4.60	2.28	1.36	4.89
Error	0.13%	1.17%	1.68%	0.81%	0.37%	1.36%
(c)	Sensor 1	Sensor 2	Sensor 3	Sensor 4	Sensor 5	Sensor 6
ToF between reflections (ns)	76.56	76.26	80.96	75.84	115.55	113.62
Thickness from ultrasound (μm)	246.14	245.18	260.28	243.81	371.49	365.30
Thickness from microscope (μm)	242.21	240.22	264.21	247.43	371.20	371.14
Deviation (μm)	3.93	4.96	3.93	3.61	0.30	5.84
Error	1.62%	2.06%	1.49%	1.46%	0.08%	1.57%
(d)	Sensor 1	Sensor 2	Sensor 3	Sensor 4	Sensor 5	Sensor 6
ToF between reflections (ns)	53.40	53.86	47.56	48.88	111.71	111.00
Thickness from ultrasound (μm)	171.68	173.15	152.92	157.14	359.15	356.85
Thickness from Microscope (μm)	185.43	179.01	153.07	160.44	359.18	358.09
Deviation (μm)	13.75	5.86	0.15	3.30	0.03	1.24
Error	7.42%	3.27%	0.10%	2.06%	0.01%	0.35%
(e)	50 μm sample 1	50 μm sample 2	100 μm sample 1	150 μm sample 1		
Nominal depth (μm)	50.00	50.00	100.00	150.00		
Ultrasound (μm)	99.25	76.74	119.54	194.28		
Microscope (μm)	98.62	80.05	122.65	189.15		

measured by thermocouple. The sensor layout and the pictures of inner surface are presented in Fig. 14.

During the test, the sample was clamped to the bearing holder and the ultrasound sensors were pressed between the bearing and holder, as shown in Fig. 14(b), which potentially led to an imbalanced local pressure, especially at the location of ultrasound sensors. As shown in Fig. 14(c), because the sensors were uniformly distributed, a relatively uniform wear on the inner surface could be observed.

### 7.2 Results

For all the ultrasound sensors in this test, the ultrasound signals were collected before and after the test, as an example of sensor 1 shown in Fig. 15. The depth of wear could be obtained by

comparing the difference before and after operation. The results of the dry-running test are shown in Table 6 and Fig. 16. The thickness of the coating could not be observed before the operation (it would have meant sectioning the bearing), so only the thickness after the operation was used for comparison.

According to the result in Table 6, the deviation and relative error values are generally around 10 μm and within 5%, with a maximum relative error of 9.47%. And regarding the wear behaviour in Fig. 16, the top side in Fig. 14(a) (the side of sensors 1, 3, 5, ...) suffered less wear compared with the other side. This may be due to an imbalance between the upper and lower rows. On the circumferential direction, it shows a larger wear in the middle, which corresponds to the loaded region, then the right side, and less wear on the left side.

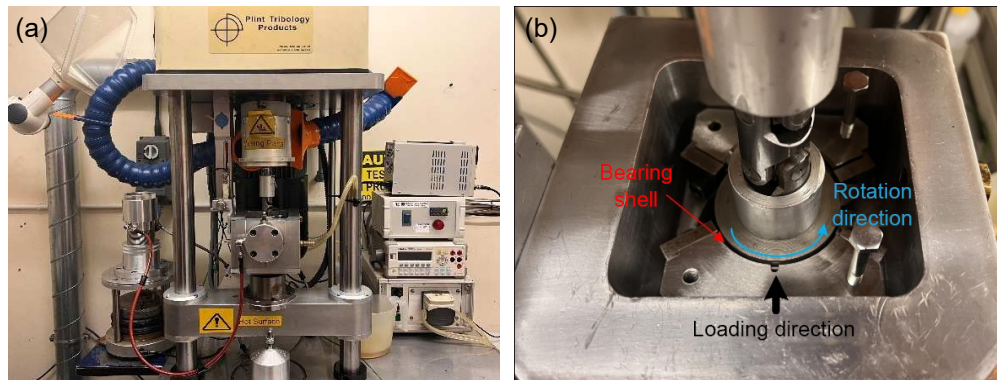


Fig. 13 (a) Rotary tribometer TE92; (b) assembly of test bearing sample.

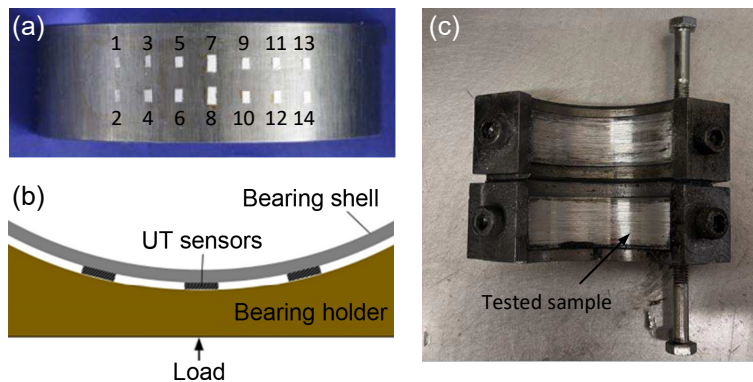


Fig. 14 (a) Instrumented aluminium alloy-coated sample for dry-running test; (b) diagram of contact between bearing holder and bearing shell; (c) damaged surface of aluminium alloy-coated sample after dry-running test.

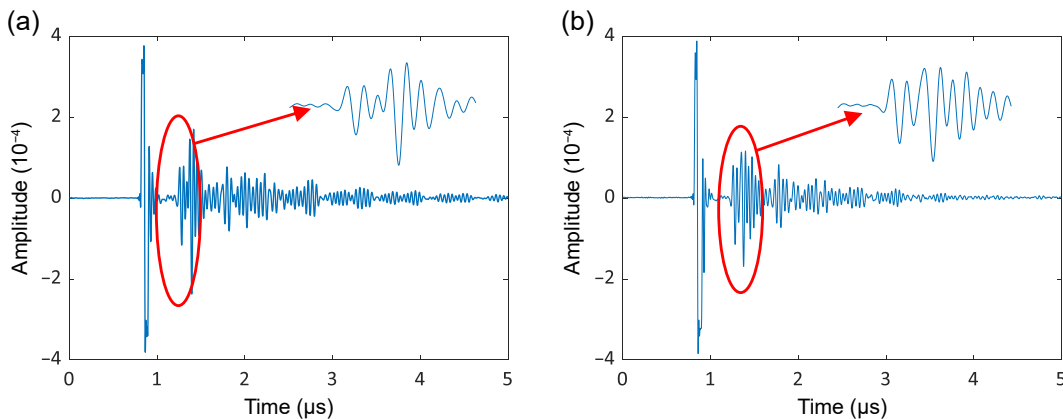


Fig. 15 Ultrasound data of sensor 1 from a bearing shell in dry-running test: (a) before dry-running; (b) after dry-running.

## 8 Discussion

### 8.1 Frequency of ultrasound sensors

In this paper, two different ultrasound frequencies are compared, 10 and 22 MHz. However, according to the experience, a higher ultrasound frequency is more suitable for precise measurement because of its shorter wavelength and higher resolution. In fact, two extra 28 MHz sensors were also investigated before the surface damage measurements. The results are shown in Table 7.

Compared with the results in Table 4, the 28 MHz sensors show a larger deviation and relative error than the 22 MHz sensors, which is contrary to expectation. This may be because of the practicalities of sensor instrumentation. Higher resonant frequency sensors consist of thinner piezo elements. The 28 MHz piezo-elements are thin, fragile, and difficult to install. Comparing the piezo-elements in Figs. 15(a) and 15(b), it shows a small gap between lead zirconate titanate (PZT) and steel, which is filled with conductive epoxy. During the bonding procedure, engineering clamps were used to make the epoxy layer as thin as possible. Because the 28 MHz PZT is fragile, during the instrumentation, the load applied on to the 28 MHz PZT was much smaller than the load on the 22 MHz PZT, led to a thicker epoxy layer on 28 MHz samples. This epoxy layer affects the phase of ultrasound and may lead to deviations in test results. Therefore, 22 MHz piezoelectric sensors were selected as the ultrasound sensor for further measurements. The microstructure of 22 and 28 MHz piezo-elements is shown in Fig. 17 and the comparison of their thicknesses is in Table 8.

### 8.2 Minimum measured thickness

In this paper, the wear depth is obtained by the thickness difference at test position before and after operation. For ultrasonic testing, theoretically, the minimum thickness that can be detected is usually equal to half of the wavelength, which can be interpreted by the signal superposition in Fig. 5. When the reflected pulses of two interfaces are exactly half a wavelength apart, the negative pressure zone of the coating–steel reflection is exactly overlapped with the positive pressure zone of the coating–air reflection. For the aluminium alloy coating, the theoretical minimum thickness detectable by ToF at 20 °C with 22 MHz ultrasound is 146 µm.

However, in some preliminary studies, when there is an extremely thin coating, the reflected signals from the two interfaces will combine into one signal. If the steel substrate is not worn, the location where the negative pressure dip of this combined signal appears represents the coating–air interface. It means that the severely worn coating can still be measured by combining the information of the coating–steel interface obtained in the unworn state. Table 9 and Fig. 18 show the test results of a severely worn aluminium-alloy bearing coating. When the measurement result shows a negative value, as sensor 3, it means the area under the tested region is fully worn.

According to the results shown in Table 9, the ultrasound ToF method is still available when the coating thickness is smaller than the theoretical limit. For sensors 1 and 4, when the actual thickness is less than 50 µm, the deviation is around 10 µm. Although it is an acceptable deviation, the relative error is around

Table 6 Results of ultrasound measurement of a bearing shell in a dry-running test

	Sensor 1	Sensor 2	Sensor 3	Sensor 4	Sensor 5	Sensor 6	Sensor 7
Ultrasound result (µm)	310.41	249.79	285.05	261.70	270.43	247.67	263.08
Microscope result (µm)	305.72	243.08	297.64	261.09	282.80	258.68	275.93
Deviation (µm)	4.69	6.71	12.59	0.61	12.37	11.01	12.86
Error	1.53%	2.76%	4.23%	0.23%	4.37%	4.26%	4.66%
Reference thickness (µm)	368.47	359.84	374.41	377.85	367.96	367.96	380.46
Wear depth from ultrasound (µm)	58.06	110.06	89.36	116.15	97.54	120.29	117.39
	Sensor 8	Sensor 9	Sensor 10	Sensor 11	Sensor 12	Sensor 13	Sensor 14
Ultrasound result (µm)	238.89	267.01	239.77	260.02	251.77	251.48	259.08
Microscope result (µm)	218.23	277.95	233.58	255.42	256.73	251.65	266.86
Deviation (µm)	20.67	10.93	6.20	4.60	4.96	0.17	7.79
Error	9.47%	3.93%	2.65%	1.80%	1.93%	0.07%	2.92%
Reference thickness (µm)	374.89	379.85	369.98	376.03	378.22	366.66	376.23
Wear depth from ultrasound (µm)	136.00	112.84	130.20	116.02	126.45	115.18	117.15

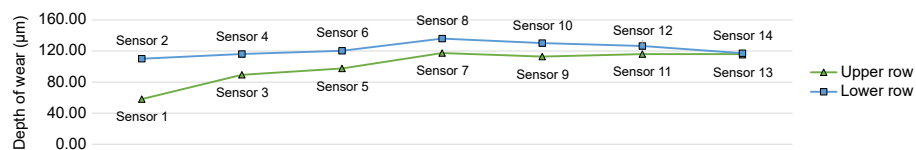


Fig. 16 Trend of wear behaviour along circumferential direction.

Table 7 Measurement results of aluminium alloy coating using 28 MHz sensors

	Sensor 1	Sensor 2
ToF between interfaces (ns)	112.52	113.78
Thickness from ultrasound (µm)	361.75	365.80
Thickness from microscope (µm)	356.43	371.45
Deviation (µm)	5.32	5.65
Error	1.49%	1.52%

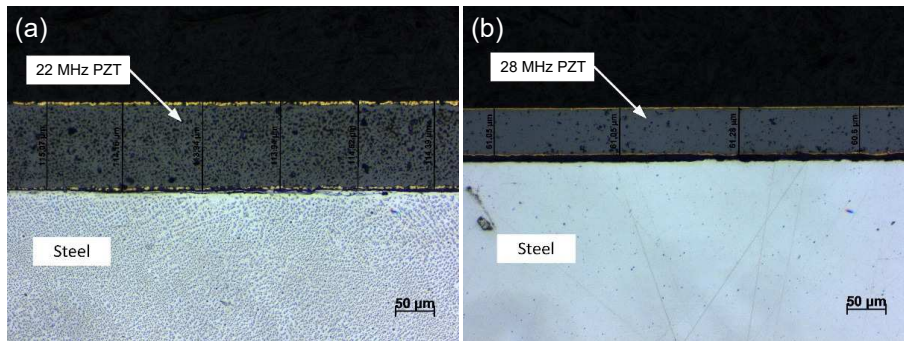


Fig. 17 Microstructure and thickness measurement of ultrasound sensors installed on bearing shell: (a) 22 MHz and (b) 28 MHz.

Table 8 Thickness of sensors with different frequencies

	Aluminium-22 MHz		Aluminium-28 MHz	
	Sensor 1	Sensor 2	Sensor 1	Sensor 2
Average (μm)	114.385	115.752	60.995	60.658

Table 9 Measurement results of aluminium alloy coating under severe running condition

	Sensor 1	Sensor 2	Sensor 3	Sensor 4
Ultrasound result (μm)	35.27	110.64	-9.88	43.54
Microscope result (μm)	46.44	103.50	—	54.00
Deviation (μm)	11.17	7.14	—	10.46
Error	24.05%	6.90%	—	19.37%

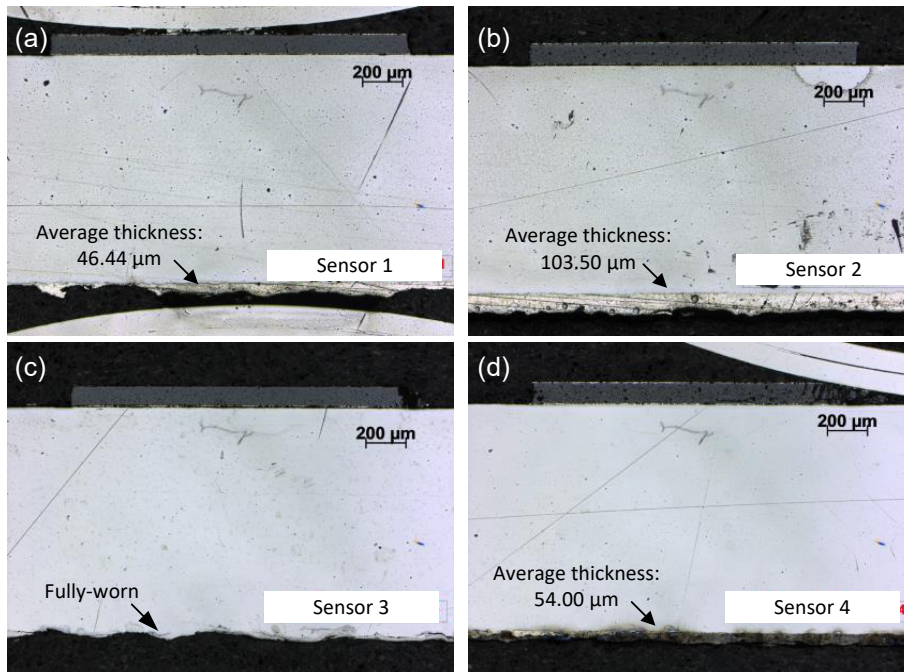


Fig. 18 An example of aluminium alloy-coated bearing shell under severe running condition. The microscope results with 5× objective: (a) sensor 1; (b) sensor 2; (c) sensor 3; (d) sensor 4.

20% due to a small actual value. In fact, wear is a dynamic process, and the coating material is gradually removed due to friction. Therefore, in the actual applications, such as a continuous measurement, the thickness reduction can be measured earlier, before it grows into severe wear. However, the appropriate data processing methods still deserve further research, in case the initial coating thickness is under the limit, and the switch between regular method and for specific cases is also a big challenge.

### 8.3 Further development

In this paper, an ultrasound-based wear measurement approach was proposed. Regarding the comparison between the ultrasound and microscope results, the microscope results were obtained from a discrete sampling, about every 100 μm along the direction

of sensors. This means that the microscope results are not a strictly absolute thickness of the coatings. However, the ultrasound measurement shows similar results with the microscope one, which means it has similar accuracy with the microscope and it can replace the microscope in specific working conditions.

In fact, during the practical operation of bearing shells, the other methods such as eddy-current or optical testing are rarely embedded into the bearing system. The ultrasound sensors with small volumes can be easily instrumented into a large system and can potentially achieve real-time measurement in practical applications. In this paper, the thickness results were compared before and after the operation using ultrasound, and the signals were collected by temporary wirings. Further research will focus

on real-time measurement using permanently instrumented sensors and more common ultrasound solutions.

## 9 Conclusions

In this paper, ultrasound-based measurement was proposed to detect the wear or the thickness reduction of the aluminium alloy coating of a journal bearing shell. Based on a series of numerical simulations, 22 MHz piezoelectric sensors were selected as working as a transmitter and receiver during the measurement. A series of experiments were performed, including measurement using different frequencies, and on bearings with artificial machined damage and damage generated in a dry running test.

The ultrasound approach shows a maximum 5.84  $\mu\text{m}$  deviation compared with the microscope result and 1.57% relative error when measuring an undamaged bearing coating (100  $\mu\text{m}$  artificially damaged sample 1, sensor 6). For the artificially damaged surfaces, the ultrasound results are very close to those of microscope, with a general deviation around 5  $\mu\text{m}$  and a maximum deviation of 13.75  $\mu\text{m}$  (7.42% relative error). Regarding the dry-running test, the deviation between ultrasound and microscope results and relative error values are generally around 10  $\mu\text{m}$  and within 5%, with a maximum relative error of 9.47%. It can be regarded that the ultrasound has similar accuracy to sectioning the shell and measuring damage or thickness with a microscope and it hopes to achieve real-time measurement in further practical applications.

## Acknowledgements

The authors would like to acknowledge the financial support of the Daido Metal Co. who funded this work. Rob Dwyer-Joyce would also like to acknowledge the financial support of the Engineering and Physical Sciences Research Council through his fellowship on Tribo-Acoustic Sensors EP/N016483/1.

## Declaration of competing interest

The authors have no competing interests to declare that are relevant to the content of this article.

## References

- [1] Glavatskih S B. A method of temperature monitoring in fluid film bearings. *Tribol Int* 37(2): 143–148 (2004)
- [2] Narendiranath Babu T, Manvel Raj T, Lakshmanan T. A review on application of dynamic parameters of journal bearing for vibration and condition monitoring. *J Mech* 31(4): 391–416 (2015)
- [3] Miettinen J, Andersson P, Wikström V. Analysis of grease lubrication of a ball bearing using acoustic emission measurement. *PI Mech Eng J—J Eng* 215(6): 535–544 (2001)
- [4] He Y Y, Zhang X M, Friswell M I. Defect diagnosis for rolling element bearings using acoustic emission. *J Vib Acoust* 131(6): 061012 (2009)
- [5] Sateesh Kumar P, Amarnath M, Kamarapu S K, Varatharajan G, Chelladurai H, Vardhaman B A, Ramkumar J. A study of surface fatigue wear and influence of contaminated lubricant in journal bearing system using tribological and vibration analyses. *PI Mech Eng E—J Pro* <https://doi.org/10.1177/09544089241233119> (2024)
- [6] Tervo J, Junttila J, Lämsä V, Savolainen M, Ronkainen H. Hybrid methodology development for lubrication regimes identification based on measurements, simulation, and data clustering. *Tribol Int* 195: 109631 (2024)
- [7] Zhang C, Liang S Y, Qiu J. Bearing failure prognostic model based on damage mechanics and vibration monitoring. *Tribol Trans* 44(4): 603–608 (2001)
- [8] Mokhtari N, Gühmann C. Classification of journal bearing friction states based on acoustic emission signals. *Tm-Tech Mess* 85(6): 434–442 (2018)
- [9] Ma J J, Zhang H, Lou S, Chu F L, Shi Z Q, Gu F S, Ball A D. Analytical and experimental investigation of vibration characteristics induced by tribofilm-asperity interactions in hydrodynamic journal bearings. *Mech Syst Signal Process* 150: 107227 (2021)
- [10] Poddar S, Tandon N. Study of oil starvation in journal bearing using acoustic emission and vibration measurement techniques. *J Tribol* 142(12): 121801 (2020)
- [11] Mo Z L, Wang J Y, Zhang H, Zeng X F, Liu H Y, Miao Q. Vibration and acoustics emission based methods in low-speed bearing condition monitoring. In: Proceedings of the Prognostics and System Health Management Conference (PHM-Chongqing), Chongqing, China, 2018: 871–875.
- [12] Aye S A. Bearing damage characterization using SVAN 958 and laser in the time domain. *AIP Conf Proc* 1457: 398–404 (2012)
- [13] Xue XH, Dong YG, Wu X. Motion induced eddy current sensor for non-intrusive vibration measurement. *IEEE Sens J* 20(2): 735–744 (2020)
- [14] Barszczewska A, Piątkowska E, Litwin W. Selected problems of experimental testing marine stern tube bearings. *Pol Marit Res* 26(2): 142–154 (2019)
- [15] Cho M R, Han D C, Choi J K. Oil film thickness in engine connecting-rod bearing with consideration of thermal effects: Comparison between theory and experiment. *J Tribol* 121(4): 901–907 (1999)
- [16] Wen B G, Ren H J, Dang P F, Hao X, Han Q K. Measurement and calculation of oil film thickness in a ball bearing. *Ind Lubr Tribol* 70(8): 1500–1508 (2018)
- [17] Beamish S, Dwyer-Joyce R S. Experimental measurements of oil films in a dynamically loaded journal bearing. *Tribol Trans* 65(6): 1022–1040 (2022)
- [18] Beamish S, Li X, Brunskill H, Hunter A, Dwyer-Joyce R. Circumferential film thickness measurement in journal bearings via the ultrasonic technique. *Tribol Int* 148: 106295 (2020)
- [19] Li W, Hu Z Q, Yang Y L, Qi X W, Zhou H L. Credibility in evaluating on-line wear-depth detection of self-lubricating spherical plain bearings. *Adv Mech Eng* 8(9): 1687814016666746 (2016)
- [20] Sharma S C, Hargreaves D. A suitable method for journal bearing wear measurement. *Ind Lubr Tribol* 66(1): 15–22 (2014)
- [21] Li H J, Liu Y, Liao H R, Liang Z R. Online measurement of wear depth based on displacement signal of vertical tester. *Tribol Int* 200: 110179 (2024)
- [22] Yang S M, Cao N, Yu B. Wear debris measurement in lubricating oil based on inductive method: A review. *Meas Contr* 56(7–8): 1422–1435 (2023)
- [23] Chasalevris A, Dohnal F, Chatzivasvas I. Experimental detection of additional harmonics due to wear in journal bearings using excitation from a magnetic bearing. *Tribol Int* 71: 158–167 (2014)
- [24] Valigi M, Logozzo S, Affatato S. New challenges in tribology: Wear assessment using 3D optical scanners. *Materials* 10(5): 548 (2017)
- [25] Netzelmann U, Walle G. High-speed thermography of thin metallic coatings. *AIP Conf Proc* 463: 401–403 (1999)
- [26] Xu N, Wang C, Yang L Q, Barimah E K, Jose G, Neville A, Morina A. Nano-scale coating wear measurement by introducing Raman-sensing underlayer. *J Mater Sci Technol* 96: 285–294 (2022)
- [27] Lu S F, Liu Z, Li D, Shen Y. Automatic wear measurement of pantograph slider based on multiview analysis. *IEEE Trans Ind Inform* 17(5): 3111–3121 (2021)
- [28] Liu B, Zhang S S, Jing J Q, Tian B, Wang Y, Shan M G, Zhong Z. Real-time *in situ* measurement method of marine sliding bearing wear based on chirped fiber Bragg grating. *Opt Eng* 63(3): 031002 (2024)
- [29] Hu F, Ning C X, Ouyang W. Ultrasonic *in situ* measurement method

and error analysis of wear of PEEK water-lubricated bearing materials. *Measurement* **214**: 112822 (2023)

- [30] Smoqi Z, Sotelo L D, Gaikwad A, Turner J A, Rao P. Ultrasonic nondestructive evaluation of additively manufactured wear coatings. *NDT E Int* **133**: 102754 (2023)
- [31] Mokhtari N, Pelham J G, Nowoisky S, Bote-Garcia J L, Gühmann C. Friction and wear monitoring methods for journal bearings of geared turbofans based on acoustic emission signals and machine learning. *Lubricants* **8**(3): 29 (2020)
- [32] Ates C, Höfchen T, Witt M, Koch R, Bauer H J. Vibration-based wear condition estimation of journal bearings using convolutional autoencoders. *Sensors* **23**(22): 9212 (2023)
- [33] Brunskill H, Harper P, Lewis R. The real-time measurement of wear using ultrasonic reflectometry. *Wear* **332**: 1129–1133 (2015)
- [34] Dou P, Yang P P, Zheng P, Jia Y P, Wu T H, Wang S, Yu M. Ultrasound enabled simultaneous measurement of coating wear depth and lubricant film thickness in a sliding bearing. *Measurement* **240**: 115602 (2025)



ultrasound and vision measurement.

**Liqun Wu** is currently on a lectureship at Tianjin University of Science and Technology, China. He received his B.Eng. degree at Tianjin University, China (2016) and M.Sc. degree at Tianjin University of Science and Technology (2019). He obtained his Ph.D. degree in tribology at the University of Sheffield, UK, funded by Daido Metal Co., Ltd. His research area involves non-destructive testing and intelligent measurement system, especially



investigating lubrication regimes, and analyzing wear and friction performance, his research interests include developing innovative solutions for condition monitoring and enhancing material performance in critical applications.

**Ion Palamarciuc** is a senior R&D engineer at Daido Metal, with his Ph.D. degree in materials engineering from Gheorghe Asachi Technical University of Iasi, Romania. His research focuses on the intersection of tribology, material science, and condition monitoring, with extensive expertise in advanced testing methods, such as acoustic emission, destructive and non-destructive evaluation techniques. With a background in developing coatings,



**Rizwan Sarwar Bajwa** is a project manager/PMO at the ENERCOMP (ARAMCO-King Abdullah University of Science and Technology (KAUST) Consortium for Nonmetallics and Composites in Energy Applications), Mechanics of Composites for Energy and Mobility Laboratory (MCEM), PSE Division, KAUST, Kingdom of Saudi Arabia (KSA). Before joining KAUST in 2024, he served as R&D Manager at the European Technical Centre, UK, for Daido Metal Co., Ltd., where he led company's research and development efforts focusing on high-performance products, materials, and innovative technologies for the automotive, marine, and energy sectors. Expert in leading cross-functional teams, driving product development from concept to commercialization. He finished his Ph.D. degree at Bournemouth University, UK, fully sponsored by Schaeffler Technologies GmbH & Co. KG., Germany. After the completion of his Ph.D. degree, he joined Daido Metal Co., Ltd., European Technical Centre, UK, in 2016.



cover a wide range of areas such as material science, surface engineering & manufacturing, tribology, and most recently, emerging technologies.

**Yi Zhang** received his Ph.D. degree in materials engineering at Loughborough University, UK, in 2007. After the completion of his Ph.D. degree, he joined Daido Metal Co., Ltd., European Technical Centre, UK, as a materials scientist in 2007, became principle materials scientist and Head of R&D in 2013, and led the research activities in UK in 2015. Since 2022, he has been working in the Corporation Headquarters in Japan. His research interests



Doctoral Training in Integrated Tribology, an EPSRC Advanced Career Fellow, Fellow of the Royal Academy of Engineering, and past editor of the *IMEchE Journal of Tribology*.

**Rob Dwyer-Joyce** is director of the Leonardo Centre for Tribology at the University of Sheffield, UK. He has a first degree in mechanical engineering and did his Ph.D. research in tribology at Imperial College, UK. He pioneered the use of ultrasound for tribological machine elements, to measure oil film, contact load, and viscosity. He has published over 150 papers in international journals. He is director of the Centre for